jmb Article

Catalytic Metal Ion Rearrangements Underline Promiscuity and Evolvability of a Metalloenzyme

Moshe Ben-David[1], Grzegorz Wieczorek[1], Mikael Elias[2], Israel Silman[3], Joel L. Sussman[1] and Dan S. Tawfik[2]

*1 - **Department of Structural Biology,** Weizmann Institute of Science, Rehovot 76100, Israel*
*2 - **Department of Biological Chemistry,** Weizmann Institute of Science, Rehovot 76100, Israel*
*3 - **Department of Neurobiology,** Weizmann Institute of Science, Rehovot 76100, Israel*

***Correspondence to Joel L. Sussman and Dan S. Tawfik:** Departments of Structural Biology and Biological Chemistry, Weizmann Institute of Science, Rehovot 76100, Israel. joel.sussman@weizmann.ac.il; tawfik@Weizmann.ac.il*
http://dx.doi.org/10.1016/j.jmb.2013.01.009
Edited by M. Guss

Abstract

Although largely deemed as structurally conserved, catalytic metal ion sites can rearrange, thereby contributing to enzyme evolvability. Here, we show that in paraoxonase-1, a lipo-lactonase, catalytic promiscuity and divergence into an organophosphate hydrolase are correlated with an alternative mode of the catalytic Ca^{2+}. We describe the crystal structures of active-site mutants bearing mutations at position 115. The histidine at this position acts as a base to activate the lactone-hydrolyzing water molecule. Mutations to Trp or Gln indeed diminish paraoxonase-1's lactonase activity; however, the promiscuous organophosphate hydrolase activity is enhanced. The structures reveal a 1.8-Å upward displacement towards the enzyme's surface of the catalytic Ca^{2+} in the His115 mutants and configurational changes in the ligating side chains and water molecules, relative to the wild-type enzyme. Biochemical analysis and molecular dynamics simulations suggest that this alternative, upward metal mode mediates the promiscuous hydrolysis of organophosphates. The upward Ca^{2+} mode observed in the His115 mutants also appears to mediate the wild type's paraoxonase activity. However, whereas the upward mode dominates in the Trp115 mutant, it is scarcely populated in wild type. Thus, the plasticity of active-site metal ions may permit alternative, latent, promiscuous activities and also provide the basis for the divergence of new enzymatic functions.

Introduction

Metal binding sites, especially those playing a catalytic role, exhibit high structural conservation.[1] The location of the metal ion and of its ligating residues perfectly superposes, even in distant superfamily members that catalyze different chemical reactions.[2–6] There exist, however, indications of changes in the configuration of catalytic metals, as part of the catalytic cycle, or upon binding different substrates.[7–12] Here, we describe the case of serum paraoxonase-1 (PON1), in which relocation of the catalytic Ca^{2+} underlies its catalytic promiscuity and divergence to a new enzymatic function.

PON1 is a member of the serum paraoxonase family that is found primarily in mammals. Our earlier work yielded a recombinant PON1 variant (rePON1), the sequence of which is 91% identical with rabbit PON1 and 86% identical with human PON1, and its kinetic parameters are essentially identical with those of human PON1.[13] This permitted the determination of the first PON1 crystal structure and, recently, of its complex with the lactone analogue 2-hydroxyquinoline (2HQ).[14] PON1 is a six-bladed β-propeller, with a central tunnel occupied with two calcium ions—a buried structural ion and a catalytic one at the active site's bottom (referred to here as Ca^{2+} or calcium ion).

PON1's native activity is the hydrolysis of lipophilic lactones, but it also promiscuously hydrolyzes organophosphates, particularly paraoxon. The enzyme uses different subsets of its catalytic machinery, and different active-site conformations, to catalyze these two reactions.[14] Nonetheless, the catalytic Ca^{2+} and its ligating residues are essential for both. The Ca^{2+}-ligating residue E53, along with

residue H115 (which resides near the Ca^{2+}, but does not directly ligate it) and H134 that forms a His dyad that increases H115's basicity, activates the hydrolytic water for the lactonase activity.[14] Mutations of H115 to Gln, or more drastically to Trp, reduce the lactonase activity by 100- to 600-fold, depending on the lactone substrate. The organophosphate hydrolase activity is, however, enhanced.[15–17] For example, the substitution of H115 to Trp yields >300-fold enhancement in the hydrolysis of parathiol, a phosphothiolate analogue of paraoxon, and enhanced hydrolysis of various nerve agents.[15,18] Indeed, the change of His115 to Trp, followed by mutations in other residues, underlies the divergence of PON1 into a highly proficient organophosphate hydrolase with no lactonase activity.[19]

Here, we describe the structural and mechanistic changes that underlie PON1's functional transition into an organophosphate hydrolase. We also propose a detailed mechanism for PON1's organophosphate hydrolase activity. Taken together with other observations of metal rearrangements,[8,10,20,21] our results suggest that the plasticity of catalytic metal ions may play a key role in the functional diversification of certain metalloenzyme families.

Results

Crystal structure of H115 mutants

We determined the crystal structure of PON1's H115W mutant, as well as of the H115Q/H134Q mutant in which both residues of the His dyad have been mutated. Both mutants exhibit a decrease in the lactonase activity, with the double mutant being practically inactive[16] (Table 1). Their organophosphate hydrolase activity, however, varies depending on the substrate, from a slight decrease relative to wild type to a significant improvement (Table 1). As in earlier studies, rePON1 was used for crystallization and for the mutational analysis. Crystals of the H115W mutant, diffracting to 2.1 Å, were obtained, as for rePON1, at pH 6.5[14] [Protein Data Bank (PDB) code: 3SRE]. The space group was the same as for the rePON1 crystals, and the unit cell parameters were very similar. Structure determination was carried out by molecular replacement, using the pH 6.5 rePON1 structure as the model. The H115Q/H134Q crystals diffracted to 2.3 Å, and their structure was determined as for the H115W mutant (Table 2).

Superimposition of the wild-type-like rePON1 and H115W structures showed no significant backbone changes (Supplementary Fig. 1a). However, a 1.8-Å upward displacement, that is, towards the enzyme's surface, of the catalytic Ca^{2+} was observed (Fig. 1a), whereas the position of the structural Ca^{2+} did not change (Supplementary Fig. 1b). The occupancy of the catalytic Ca^{2+} at its new position was ~60%, compared to 100% in wild-type-like rePON1, and the bound phosphate ion present in the latter is absent. The remaining 40% occupancy may correspond to weak density at the wild-type Ca^{2+} position. However, the distances, the weak density, and the ligation geometry fit a water molecule[22] (Supplementary Fig. 2). The residues coordinating the

Table 1. Kinetic parameters for wild-type-like rePON1 and its mutants

His115			115 mutants		
rePON1	Paraoxonase	Lactonase[a]	rePON1	Paraoxonase	Lactonase[a]
Wild type			*H115W*		
k_{cat} (s^{-1})	5.0±0.6	190±16	k_{cat} (s^{-1})	7.3±0.2 (↑ 1.4)	0.13±0.01 (↓ 1451)
K_m (mM)	2.3±0.3	1.1±0.1	K_m (mM)	1.6±0.1 (↓ 1.5)	0.50±0.01 (↓ 2.4)
k_{cat}/K_m ($M^{-1}s^{-1}$)	2150±300	169,100±18,000	k_{cat}/K_m ($M^{-1}s^{-1}$)	4700±250 (↑ 2.2)	290±4 (↓ 577)
N224D			*H115W/N224D*		
k_{cat} (s^{-1})	0.150±0.009 (↓ 33)	1.50±0.06 (↓ 127)	k_{cat} (s^{-1})	1.15±0.06 (↓ 6.4)[b]	0.08±0.01 (↓ 1.6)[b]
K_m (mM)	2.9±0.1 (↑ 1.3)	1.00±0.05 (↓ 1.1)	K_m (mM)	2.3±0.2 (↑ 1.5)[b]	0.75±0.09 (↑ 1.5)[b]
k_{cat}/K_m ($M^{-1}s^{-1}$)	50±2 (↓ 42)	1460±120 (↓ 116)	k_{cat}/K_m ($M^{-1}s^{-1}$)	492±23 (↓ 9.5)[b]	115±2 (↑ 2.6)[b]
E53Q[c]			*H115Q*		
k_{cat} (s^{-1})	ND[d]	0.130±0.003 (↓ 1451)	k_{cat} (s^{-1})	1.10±0.03 (↓ 4.5)	1.2±0.1 (↓ 157)
K_m (mM)	ND[d]	0.180±0.006 (↓ 6.4)	K_m (mM)	1.80±0.07 (↓ 1.3)	0.80±0.03 (↓ 1.4)
k_{cat}/K_m ($M^{-1}s^{-1}$)	1.30±0.08 (↓ 1692)	750±12 (↓ 226)	k_{cat}/K_m ($M^{-1}s^{-1}$)	630±43 (↓ 3.4)	1500±170 (↓ 113)
D269N[c]			*H115Q/H134Q*[e]		
k_{cat} (s^{-1})	0.090±0.002 (↓ 56)	0.35±0.01 (↓ 555)	k_{cat} (s^{-1})	4.7±0.1 (↓ 1.1)	1.75±0.05 (↓ 108)
K_m (mM)	1.10±0.02 (↓ 2.1)	0.200±0.001 (↓ 5.6)	K_m (mM)	1.20±0.07 (↓ 1.9)	1.80±0.09 (↓ 1.6)
k_{cat}/K_m ($M^{-1}s^{-1}$)	80±1 (↓ 27)	1670±34 (↓ 101)	k_{cat}/K_m ($M^{-1}s^{-1}$)	3980±180 (↑ 1.9)	965±1 (↓ 175)

[a] The chromogenic lactone substrate TBBL was used for measuring the lactonase activity. Data with other lactones are available in Ref 16.

[b] Denoted in parentheses is the fold of increase or decrease relative to the wild-type-like rePON1, unless noted with the footnote (b) is relative to the H115W mutant.

[c] No activity was observed for the H115W/E53Q and H115W/D269N mutants above the background rates at maximal enzyme concentrations (25 μM), thus setting a detection threshold of $k_{cat}/K_m \sim 1\ M^{-1}s^{-1}$ for TBBL and $k_{cat}/K_m \sim 0.1\ M^{-1}s^{-1}$ for paraoxon.

[d] Not determined.

[e] Taken from Ref 16.

Table 2. Summary of data collection and refinement statistics

	H115W	H115Q/H134Q
Data collection		
Resolution range (Å)[a]	50–2.1 (2.18–2.10)	40–2.3 (2.38–2.3)
Space group	$P4_32_12$	$P4_32_12$
Unit cell dimensions (Å)		
$a=b$	93.8	93.7
c	145.2	144.6
Number of reflections measured	357,550	396,164
Number of unique reflections[a]	36,561 (3785)	27,832 (2860)
R_{sym}[a]	0.099 (0.59)	0.086 (0.52)
Completeness (%)[a]	100 (99)	100 (100)
Redundancy[a]	9.3 (7.2)	13.5 (8.7)
$\langle I\rangle/\langle\sigma(I)\rangle$[a]	26.12 (3)	30.9 (4.2)
Refinement statistics of the current models		
R_{free} (%)	21.2	21.8
R_{work} (%)	18.4	17.8
Water molecules	171	147
r.m.s.d.		
Bond length (Å)	0.029	0.029
Bond angles (°)	2.335	2.191
Ramachandran plot		
Most favored regions (%)	83.5	84.8
Additionally allowed regions (%)	15.8	14.2
Generously allowed regions (%)	0.7	1.1
Disallowed regions (%)	0	0
PDB code	4HHO	4HHQ

[a] Values in parentheses are for the highest-resolution shell.

catalytic Ca^{2+} are also altered in the mutant structure (Fig. 1b and c)—the side chains of N168, N224, and N270 do not interact directly with the catalytic Ca^{2+} as in the wild-type structure, but through waters that are absent in the native structure. The side chain of N224 also exhibits a different orientation. For E53, which retains its direct interaction with the catalytic Ca^{2+}, an alternative side-chain conformation was detected at ~30% occupancy (Supplementary Fig. 3a). Finally, the side chains of H134 and L69 also moved, thus accommodating the bulkier W115 (Supplementary Fig. 3b).

In the apo rePON1 crystal structures (PDB codes: 1V04 and 3SRE), a phosphate ion that interacts with the catalytic Ca^{2+}, and with H115's side chain, [14,23] was observed, even though phosphate was not added during purification or crystallization.[14] That the bound phosphate was not observed in the crystal structure of the Trp mutant (and Gln115, below) raises the possibility that the movement of the catalytic Ca^{2+} is related to the absence of phosphate. However, attempts to soak in phosphate to H115 mutants' crystals failed to produce a complex with phosphate ion. Further, unlike rePON1, none of the crystal structures of PON-like enzymes have a bound phosphate ion, yet the binding mode and position of their catalytic Ca^{2+} are identical with that of rePON1 (see Discussion). It is therefore unlikely that the shift in the calcium's position relates to the presence or absence of phosphate in the crystals. As is the case with 2HQ, it seems that what abolishes the binding of phosphate in the H115 mutants is the upward positional shift of the catalytic Ca^{2+}.

The crystal structure of the H115Q/H134Q mutant exhibited features similar to those of H115W (Fig. 1d). In both mutants, the side chain of residue 115 changes its orientation significantly, such that the amine of the Gln amido group overlaps with the Trp imine group (Supplementary Fig. 3c and d). The catalytic Ca^{2+} displays essentially the same location and coordination pattern as the H115W mutant (Fig. 1). In the H115Q/H134Q mutant, Q134 is reoriented towards the surface rather than towards the side chain of 115. Thus, the His dyad, whereby His134 aligns and activates His115 that serves as the catalytic base for lactone hydrolysis, is completely lost, as is the lactonase activity.

Metal ion and inhibitor binding

Earlier studies on human and rabbit PON1 had shown that the affinity of the structural Ca^{2+} is more than 2 orders of magnitude greater than that of the catalytic Ca^{2+}.[24] The loss of the structural Ca^{2+} (by prolonged ethylenediaminetetraacetic acid treatment) results in irreversible loss of activity, probably due to misfolding. The affinity measurements described here were based on reversible binding and gain of activity and, therefore, relate to the catalytic Ca^{2+} only. At low ionic strength, the apparent K_d values for the catalytic Ca^{2+} in human and rabbit PON1 are both ~3 μM,[24] and rePON1 displays a similar value (Supplementary Table 1). As for other Ca^{2+} enzymes,[25] an increase in the ionic strength (i.e., increasing salt concentration in the metal binding buffer to 300 mM) significantly increases K_d (100 μM; Supplementary Table 1). The H115W mutant shows 3-fold lower affinity at low ionic strength (9 μM) but nearly wild-type affinity at high ionic strength (Supplementary Table 1). Differences were also observed in the displacement of the catalytic Ca^{2+} by other metal ions.[24] Of the metal ions tested, only Sr^{2+} maintained the paraoxonase activity, both in wild-type-like rePON1 and in H115W. Other metals had an inhibitory effect (e.g., Ba^{2+}, Mg^{2+}, and Cu^{2+}). The inhibition patterns observed are in line with the catalytic Ca^{2+} being relocated, and less tightly bound, in H115W. For example, the IC_{50} for Mg^{2+} is ~620 μM for rePON1 *versus* ~100 μM for H115W (Supplementary Fig. 4).

Mutation of H115 to either Trp or Gln also abolished 2HQ binding (Supplementary Fig. 5). 2HQ is a lactone analogue and a micromolar inhibitor of PON1 that interacts tightly with the catalytic Ca^{2+}. In rePON1's structure, the distance

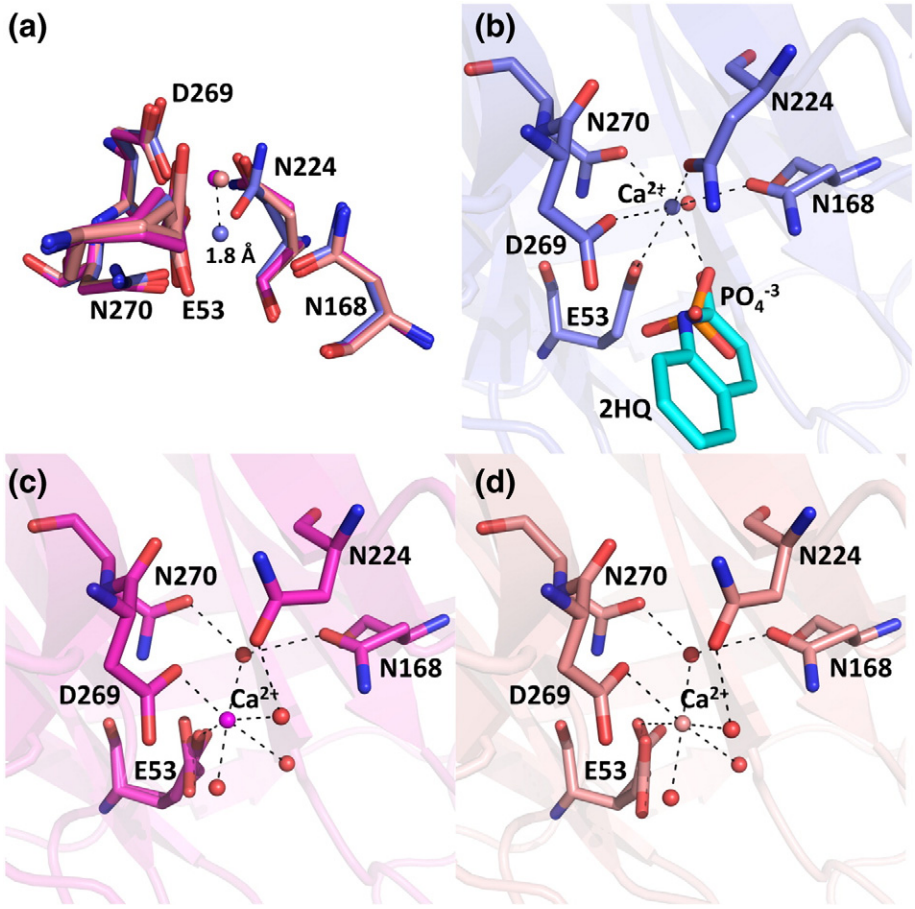

Fig. 1. Structural changes observed in H115 mutants. (a) Overlay of the catalytic Ca^{2+}-binding sites of rePON1 (blue; PDB code: 3SRE) and of the H115W (magenta) and H115Q/H134Q (salmon) mutants, illustrating the side chain and metal ion movements induced by the mutations. (b) Close-up of the catalytic Ca^{2+}-binding site of rePON1 (pH 6.5) in the presence of either phosphate (PDB code: 3SRE) or the lactone analogue 2HQ (PDB code: 3SRG). (c) Close-up of the catalytic Ca^{2+}-binding site of the H115W mutant. (d) Close-up of the catalytic Ca^{2+}-binding site of the H115Q/H134Q mutant. Red spheres represent water molecules.

between Ca^{2+} and 2HQ's lactam's carbonyl oxygen is 2.4 Å (Fig. 1b). 2HQ is also H-bonded to the side chains of H115, N168, and D269.[14] The H-bond between 2HQ and H115 could be maintained upon mutation of H115 to Gln. It is therefore plausible that the H115Q mutant lost its capacity to bind 2HQ primarily due to changes in the location of the catalytic Ca^{2+} and its ligating residues.

Mutational analysis of the Ca^{2+}-ligating residues

The repositioning of the catalytic Ca^{2+} should also be manifested in mutations in the coordinating residues exhibiting different effects upon wild-type-like rePON1 *versus* the H115W activity and/or on lactonase *versus* paraoxonase activity. Site-specific saturation mutagenesis, that is, replacement of a given residue by all the other 19 amino acids, was applied to all the residues coordinating the catalytic Ca^{2+}: D269, E53, N168, N224, and N270. A parallel set of saturation libraries was constructed for the H115W mutant. Multiple replacements in the same position, and parallel examination of the lactonase and paraoxonase activities, allowed us to distinguish (i) global effects (complete loss of activity due to loss of the bound Ca^{2+}) from local ones (a role in the catalysis of one activity but not of the other) and (ii) differences in the Ca^{2+}-ligating modes of the wild-type-like rePON and the H115W mutant.

The N224 saturation library yielded active variants. However, the effects of the mutations were similar for both substrates, suggesting that N224 plays a similar role in both the lactonase and paraoxonase activities (Supplementary Fig. 6c). Active N224 mutants of rePON1 included N224V and N224A, in which the potential to interact with the Ca^{2+} is abolished. However, for H115W, activity was observed only in the N224 to Asp, Thr, and Ser mutants, where the potential to interact with the catalytic Ca^{2+} via a water molecule is retained (Fig. 1c). When tested with

paraoxon, the most active mutant in the N224 library, N224D, exhibited an ~5-fold larger effect on k_{cat} in rePON1 relative to its effect in H115W (Table 1). These observations are in agreement with the observed switch in the mode of Ca^{2+} binding, from a direct interaction in the wild type to a water-bridged interaction in H115W (Fig. 1b and c).

The rePON1 N270 substitution library displayed a similar number of active variants with both paraoxon and TBBL (Supplementary Fig. 6d), suggesting that this residue plays a similar and relatively minor role in catalysis for both substrates. The N270Q mutations had a minor effect (<2-fold decrease) on rePON1's paraoxonase and lactonase activities and a similarly minor effect on H115W's paraoxonase activity (H115W shows negligible lactonase activity). Even the N270G mutants of rePON1 and H115W displayed ~7% activity. Indeed, certain PON1-related enzymes have a glycine at the corresponding analogue positions (Supplementary Fig. 10).

In the N168 saturation libraries of both rePON1 and H115W, only the N168Q mutants displayed substantial activity (2–5% activity relative to N168; Supplementary Fig. 6b). Since all the mutants are inactive except for N168Q, and the mutations similarly affect the lactonase and paraoxonase activities (in rePON1), N168 seems to be crucial primarily for Ca^{2+} binding.

E53 and D269 maintain direct interactions with the catalytic Ca^{2+} in both rePON1 and H115W (Fig. 1c). As earlier proposed,[14,26] these residues also play a critical role in catalysis. Indeed, as already reported for D269,[16] the E53 substitution library yielded only inactive mutants at the level of detection in crude lysates. Since much lower activities can be detected using purified enzymes, the conservative mutants D269N and E53Q were purified and assayed at high protein concentrations. The rePON1 E53Q and D269N mutants both showed measurable lactonase and especially paraoxonase activity. However, both mutations resulted in complete loss of the paraoxonase activity in H115W (Table 1).

Overall, the differences in the effects of D269N and E53Q on the wild-type-like rePON1 *versus* H115W, and the opposite trend for N224D, are in agreement with the observed changes in the location and coordination mode of the catalytic Ca^{2+}. The similar effects of mutations in 224, 168, and 270 on both the lactonase and paraoxonase activities suggest that these residues' primary role is ligation of the Ca^{2+}. In contrast, E53 and D269 show different effects on the lactonase *versus* the paraoxonase activity, suggesting that, in addition to ligating the Ca^{2+}, they may play specific roles in catalysis. Indeed, E53 seems to cooperate with H115 in aligning and activating the attacking water molecule for lactonase hydrolysis, and D269 may assist in coordinating the alkoxide leaving group (Fig. 9 in Ref. 14). Conversely, as discussed below, E53, in cooperation with D269, seems to align and activate the attacking water for paraoxon hydrolysis in both wild type[14] and H115W.

Molecular dynamics simulations

The alternative Ca^{2+} mode seen in H115W's crystal structure, together with the biochemical data presented above, suggests that PON1 uses one Ca^{2+} mode for its native lactonase activity and a different one for its promiscuous organophosphate hydrolase activity. Although we have solved the structure of a complex of rePON1 with a lactone analogue,[14] all our attempts to obtain an organophosphate complex have, so far, failed, including co-crystallization of non-hydrolyzable analogues (e.g., phenyl- and benzyl-diethyl phosphate, and amidophosphoesters) and of organophosphate substrates with inactive mutants (D269N, E53Q). We sought, therefore, to assess the binding mode of the catalytic Ca^{2+} in organophosphate complexes of both wild-type-like rePON1 and its H115W mutant using molecular dynamics (MD) and steered molecular dynamics (SMD) simulations.

We aimed to perform simulations in a largely unbiased manner. Thus, having proposed a mechanism for PON1's action on paraoxon, the SMD assessed a range of possible catalytic modes. The presumed mechanism[14,26]—water activation by the general-base action of E53 and D269—was examined as mechanism #6 (*m6*). Alternative mechanisms included action of E53 alone as a general base or nucleophile (*m1*) and the nucleophilic action of D269 (*m2*). Furthermore, although a mutagenesis study appeared to have ruled out their direct involvement in catalysis,[16] we examined models for general-base catalysis of paraoxon hydrolysis by three active-site residues that do not ligate the Ca^{2+}: D183 (*m3*), H115 (*m4*, for wild type), and H285 (*m5*). The seventh mode tested for wild type (*m7*) corresponded to water activation by the joint action of E53 and H115, that is, the proposed lactonase mechanism.[14] The seven putative modes were rendered as sets of geometric criteria: distances, angles, and dihedrals between the relevant atoms in the active-site residues and in paraoxon. The structural models obtained by repeated SMD/MD simulations were categorized according to whether the structural criteria for a given mechanism were met or not. Simulations in which the SMD trajectory resulted in a catalytically relevant mode of binding of paraoxon were defined as a "hit".

Modes *m3* to *m5*, which are in more likelihood irrelevant, gave essentially no hits (Supplementary Table 2), thus supporting the validity of the simulations. For wild type, modes *m1* and *m7* achieved the highest scores, whereas for H115W, *m6* scored the highest. Common to all three modes is the participation of E53. Indeed, the E53Q mutation severely

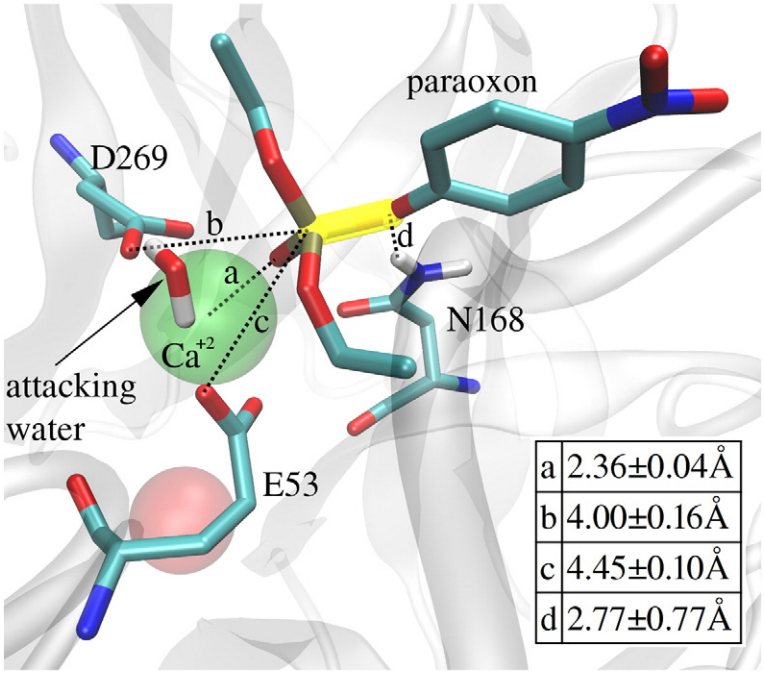

Fig. 2. A representative snapshot of mechanism *m6* from the MD simulations. Paraoxon is shown bound in the active site of the H115W mutant. E53 and D269 coordinate a water molecule that is aligned against the sessile bond linking the phenoxide oxygen of the *p*-nitrophenol leaving group to the phosphorus atom (shown with a yellow halo). The side chain of N168 appears to align the leaving group. The inset table shows the average lengths for the dotted distances, and the standard deviations, calculated from 5517 independent MD frames that resulted in paraoxon complexes that met the criteria of mechanism *m6*. The distances, angles, and dihedral angles defining all seven mechanisms are listed in Supplementary Table 3.

affects PON1's activities, especially its paraoxonase activity (Table 1). While E53 plays a critical role in the catalysis of paraoxon, the simulations suggest that it is not acting alone, but with the assistance of either H115 (for wild type, *m7*) or D269 (for H115W, *m6*). Mutations at position 115 thus shift additional weight towards D269, thereby compensating for the loss of H115 (Supplementary Table 2). For H115W, *m6* is the most probable mechanism. Accordingly, the geometry of paraoxon binding is consistent with the phosphorus atom being attacked by a water molecule that is coordinated to and activated by both D269 and E53 (Fig. 2). This mode of catalysis is also supported by the alternative conformation of E53's side chain that points towards D269 (Supplementary Fig. 3a). In the *m6* model, the side chain of N168 appears to align the leaving group. The effects of the D269N, E53Q, and N168Q mutations are all consistent with the *m6* catalytic mode, as are simulations performed by others.[26]

The SMD simulations are also consistent with standard docking models obtained for rePON1.[14] These indicated that paraoxon cannot bind in a catalytically productive mode within the active-site configuration of the 2HQ/rePON1 complex (Supplementary Fig. 7a). Rather, the rearrangement of the flexible active-site loop provides an alternative configuration into which paraoxon docks in (Supplementary Fig. 7b). Mutagenesis data also indicated that residues in this loop, primarily 71 and 74, play a role in binding paraoxon in a catalytically productive fashion.[14] In the present study, the SMD simulations were run starting from the lactone-bound active-site configuration. For the H115W mutant in which the flexible loop is disordered, the loop was first modeled in the lactone-bound conformation. Then, energy minimization was performed, followed by a short MD equilibration. In all the catalytically relevant models with paraoxon (whether in mode *m6* or any other), the active-site loop was rearranged. Specifically, the side chains of residues 71–74 had changed their orientation relative to the lactone-bound conformation (Supplementary Fig. 7b).

Finally, the simulations show that paraoxonase activity involves relocation of the catalytic Ca^{2+} relative to its position in the lactone-bound state. The upward Ca^{2+} position seen in the H115W structure is scarcely populated in the wild-type simulations (Fig. 3 and Supplementary Fig. 8). Nonetheless, the average position of Ca^{2+} deviates upward from those seen in the crystal structures of rePON1 with either phosphate or 2HQ (Fig. 3a). Furthermore, the upward positions observed for rePON1 and H115W in the simulations overlap (Fig. 3a and Supplementary Fig. 8). Tighter distributions of Ca^{2+} positions were observed, particularly for wild type, in the subset of simulations that led to catalytically productive complexes. For the H115W mutant, however, the catalytically relevant subset comprises the most frequently represented location (Fig. 3b and c). Further, in the catalytically relevant subset, the average catalytic Ca^{2+} location in the wild type nearly overlaps the upward location seen in the H115W simulations as well as in the actual H115W structure (Fig. 3). Recently performed MD simulations by another group on computational models of H115 mutants also observed upward shifts in the catalytic Ca^{2+} position and rotameric changes in its

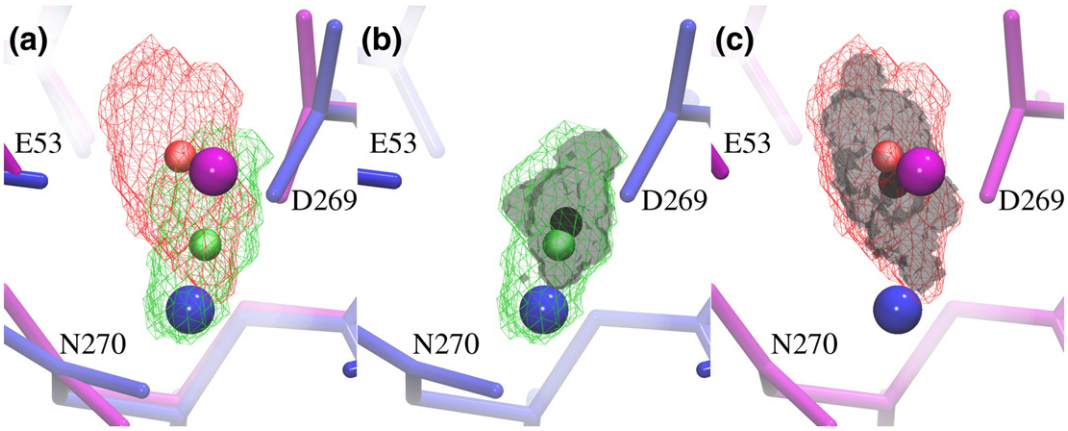

Fig. 3. Positions of the catalytic Ca^{2+} observed in crystal structures of H115W and of the wild-type-like rePON1 in complex with the lactone analogue (2HQ) and in SMD simulations. (a) The stick models represent the relevant residues in the H115W mutant (magenta) and in the complex (blue), and the large spheres, similarly color coded, represent the Ca^{2+} in the two structures. 2HQ is omitted for the sake of clarity. The red and green wireframes represent the space accessed by the Ca^{2+} during all MD simulations, for H115W and the wild-type-like rePON1complex, respectively. The small spheres, similarly color coded, show the average position for all simulations. (b) The crystal structure and the MD simulation space available for the Ca^{2+} in the wild-type-like rePON1 complex are shown as in (a); the simulation space for the subset of simulations in which paraoxon was found to bind in a mode that meets the criteria of all E53-driven mechanisms (*m1*, *m6*, and *m7*) is superimposed as a gray cloud, with the average position of the Ca^{2+} shown by a small black sphere. (c) A similar representation to that in (b) for H115W, with the simulation space displaying the subset of simulations in which paraoxon was bound in a mode meeting the criteria of mechanisms *m1* and *m6*.

ligating residues (D. Mata, C. Hadad, D. Cerasoli, and T. Magliery, submitted for publication). These independently performed studies provide further support for the models proposed here.

Discussion

The present study reveals that PON1 accommodates two alternative locations and coordination modes for its catalytic Ca^{2+} and that these modes may be used to catalyze two different reactions. PON1's native lactonase activity occurs within the canonical coordination scheme and Ca^{2+} location observed not only in PON1 but also in related lactonases that are highly divergent in sequence (Supplementary Figs. 9 and 10). The promiscuous organophosphate hydrolase activity, however, seems to utilize a different Ca^{2+} mode and a different mechanism (Fig. 2). This alternative mode that is scarcely populated in wild-type rePON1 becomes dominant upon mutating H115 and thus underlies PON1's divergence from a lactonase to an organophosphate hydrolase (Fig. 3).

We recently suggested that PON1's promiscuity stems from a coincidental overlap between the transition state for the native lactone hydrolysis and the ground state for the promiscuous substrate, paraoxon.[14] This overlap seems to be maintained irrespective of the repositioning of the catalytic Ca^{2+} and to drive paraoxon's alignment for catalysis within PON1's active site (Supplementary Fig. 11). However, as shown here, catalysis of paraoxon hydrolysis also involves an alternative mode of the catalytic Ca^{2+} and its ligating residues.

Structural conservation of the positions of the metal ion and of its ligating residues seems to prevail in most metalloenzyme families and superfamilies.[1–6] For example, in the group of PON-like structures, the Ca^{2+} of distantly related enzymes ($\leq$20% sequence identity) superpose within $\leq$0.5 Å (Supplementary Figs. 9, 10, and 12). There are, however, exceptions to this rule, namely, families in which the locations are more widely distributed (>1.4 Å; e.g., Supplementary Fig. 12a, d, and e). Aside from technical inaccuracies (e.g., low resolution and refinement), variations in metal ion positions seem to stem from variations in the ligating residues as well as from the availability of structures of distant members (Supplementary Fig. 12a).

Perhaps the best-studied example of metal ion plasticity is that of xylose isomerase, in which the catalytic Mg^{2+} (M2) shows significant positional variation. Variations were observed in the absence and presence of ligands, using X-ray[8,27–29] and neutron[30] crystallography, as well as computational simulations[31,32] (Supplementary Fig. 12d). Binding of ligands induces, on average, 1.5-Å movements of M2. The interaction with some of the ligating residues is retained, but others are replaced by waters,[28] just as we observed here in the H115 mutants (Fig. 1). Interestingly, mutations in M2's ligating residues change the enzyme's specificity, possibly by shifting the conformational equilibrium to

favor M2's alternative positions.[20,21,28] Other examples of catalytic metal ion plasticity include L-rhamnose isomerase,[12,33] alcohol dehydrogenase,[7] bacterial tyrosinase,[11] sorbitol dehydrogenase,[10] and metallo-β-lactamases.[34]

Altogether, it appears that metal ions and their coordinating side chains and water molecules can exhibit considerable plasticity. Alternative coordination modes may underlie different steps along the catalytic cycle.[7–9,35] They can also promote promiscuous binding of ligands that an enzyme has not been selected for[10] (Supplementary Fig. 12e) or catalytic promiscuity as illustrated here for PON1. Alongside the conformational diversity of the protein's backbone and side chains,[36] metal repositioning may, therefore, contribute to the catalytic versatility of enzymes and to the ease by which new enzymatic functions diverge.

That shifts in metal position and coordination have thus far been rarely observed may be due to the highly restricted sampling of natural enzyme diversity. For example, we are as yet unaware of a natural PON family member that is not a lactonase, let alone of one that is an organophosphate hydrolase. Other natural metallo-organophosphate hydrolases, however, are known, which most likely diverged from lactonases.[37,38] Analysis of the binuclear metal binding sites of methyl parathion hydrolase with the related quorum-quenching lactonase AiiA (metallo-β-lactamase superfamily) reveals a slight shift of ~0.5 Å in the position of one metal ion (Supplementary Fig. 13a). Comparison of the bacterial phosphotriesterase (PTE) and the related PTE-like-lactonases (Supplementary Fig. 13b) reveals absolute conservation of the two metal ions and their ligating residues. On the other hand, many enzymes in the amidohydrolase superfamily have only one catalytic metal, indicating evolutionary transition(s) between mono- and binuclear catalytic centers,[39] and laboratory evolution of PTE has led to changes in the metal coordination state.[40]

In a broader context, the shift indicated by the MD simulations, from a rarely populated metal state in the wild type to a dominant state in H115W (Fig. 3 and Supplementary Fig. 8), follows a general hypothesis whereby evolution capitalizes on stochastic variations, be they atomic as with PON1's alternative location of the Ca^{2+}, cellular (e.g., transcriptional noise), or organismal. Mutations do not create something from nothing. Rather, they shift the distribution such that a marginal, noise phenomenon becomes the norm.[41]

Materials and Methods

rePON1 variants and kinetics

Expression and purification of the recombinant variant used for crystallization, rePON1-G2E6, and of its mutants, were performed as previously described.[14] Purity was monitored by SDS-PAGE. RePON1-G2E6's mutants were generated by "inverse PCR"[16] and verified by DNA sequencing. The construction of the saturation libraries and their screening for lactonase (TBBL) and paraoxonase (paraoxon) activities were performed as previously described.[16] For the kinetic measurements, the concentrations of these substrates were in a range from $0.3\times K_m$ up to $(2–3)\times K_m$. k_{cat}, K_m, and k_{cat}/K_m were obtained by fitting the data to the Michaelis–Menten model with PRISM (GraphPad Software). In cases in which substrate solubility was limiting, k_{cat}/K_m values were extracted from linear fits. The pH 8.0 buffer used for enzyme kinetics contained 1 mM $CaCl_2$, 0.03% *n*-dodecyl-β-D-maltoside, 50 mM Tris, and 150 mM NaCl. All data presented are the means of ≥2 independent experiments, and the error ranges represent the standard deviation from the mean.

Metal ion affinity measurements

The dissociation constants of the catalytic Ca^{2+} for both rePON1 and the H115W mutant were determined as previously described.[24] Briefly, PON1 samples were extensively dialyzed against a buffer devoid of Ca^{2+}, 0.03% *n*-dodecyl-β-D-maltoside, and 50 mM Tris, pH 8.0, at three different NaCl concentrations (0, 150, and 300 mM) and then passed through a Chelex-100 column. Prior to activity determination, these samples were preincubated in the appropriate above-mentioned dialysis buffer (i.e., with different slat concentrations) with various $CaCl_2$ concentrations ranging from 1×10^{-2} to 5×10^{3} μM, for 1–3 h to reach equilibrium. Paraoxon (2 mM) was then added, and the apparent K_d values were derived from the Ca^{2+} concentrations required to regain 50% of the maximum enzymatic activity. For the metal inhibition studies, we used the following metal salts: $MgCl_2$, $SrCl_2$, $CuCl_2$, and $BaCl_2$, in concentrations ranging from 0.1 to 5 mM.

Crystallization, data collection, and refinement

Concentrated solutions of both the H115W and H115Q/H134Q mutants (5–10 mg/ml) were crystallized as previously described.[14] Briefly, crystals formed using the hanging drop vapor diffusion method, whereby the protein sample was mixed with equal volumes of the precipitant buffer containing 20% polyethylene glycol 3350, 0.2 M NaBr, and 0.1 M 2-[bis(2-hydroxyethyl)amino]-2-(hydroxymethyl)propane-1,3-diol propane, pH 6.5 (incubation at 19°C). Complete data sets for H115W and H115Q/H134Q were collected on beamline ID-14-1 at the European Synchrotron Radiation Facility (Grenoble, France). The diffraction images were indexed, integrated, and scaled using the HKL2000 program package.[42] Structure determination was carried out by molecular replacement (Phaser, CCP4[43]) using the published pH 6.5 structure (PDB code: 3SRE). All steps of atomic refinement were carried out with CCP4/Refmac5.[44] The model was built into $2F_o-F_c$ and F_o-F_c maps using the program Coot.[45] Both the mutants did not display well-defined electron density for the first ~20 residues at the N-terminus, as well as for the active-site flexible loop (residues 70–81),

as had already been observed for the rePON1 apo structures. Both structures contain one molecule of *n*-dodecyl-β-D-maltoside, with density corresponding to the sugar moiety seen on the enzyme's surface. Details of data collection and refinement statistics are displayed in Table 2. Figures depicting structures were prepared using PyMOL[46] and VMD.[47]

MD simulations

A new computational docking procedure was developed in order to permit thorough sampling of the possible orientations of paraoxon within the active site of PON1. Using SMD,[48] a minimized model of paraoxon was pulled into the active site of PON1 starting from a random orientation above the catalytic Ca^{2+}. The steering force was applied to the phosphoryl oxygen of the paraoxon with the catalytic Ca^{2+} serving as the reference group. After the SMD pulling procedure had been completed, the model of the paraoxon/PON1 complex was subjected to an MD simulation of 1-ns duration.[49] All the SMD and MD simulations were performed using GROMACS.[50] The entire SMD/MD procedure was repeated several hundred times for both wild-type PON1 and the H115W mutant. In the final MD run, the protein was fully flexible, which permitted examination of the conformational diversity of rePON1 in the presence of the ligand in different orientations.

Accession numbers

Coordinates and structure factors of the H115W and H115Q/H134Q mutants have been deposited in the PDB under accession numbers 4HHO and 4HHQ, respectively. An Interactive 3D Complement page appears in Proteopedia for this study.[1]

Acknowledgements

We are grateful to the Israel Structural Proteomics Centre for access to its protein purification and crystallization facilities. We thank Tom Magliery and Chris Hadad (Ohio State University) for sharing their preliminary results and for fruitful discussions. Financial support by the National Institutes of Health (2-U54-NS058183), the Defense Threat Reduction Agency (HDTRA1-11-C-0026), and the Benoziyo Center for Neuroscience are gratefully acknowledged. D.S.T. is the Nella and Leon Benoziyo Professor of Biochemistry. J.L.S. is the Pickman Professor of Structural Biology.

Supplementary Data

Supplementary data to this article can be found online at http://dx.doi.org/10.1016/j.jmb.2013.01.009

Received 10 November 2012;
Received in revised form 3 January 2013;
Accepted 7 January 2013
Available online 11 January 2013

Keywords:
catalytic calcium;
metal catalysis;
enzyme catalysis;
catalytic promiscuity;
conformational diversity

† http://proteopedia.org/wiki/index.php/Journal:JMB:3

Abbreviations used:
PON1, paraoxonase-1; rePON1, recombinant PON1 variant; 2HQ, 2-hydroxyquinoline; PDB, Protein Data Bank; MD, molecular dynamics; SMD, steered molecular dynamics; PTE, phosphotriesterase.

References

1. Torrance, J. W., Macarthur, M. W. & Thornton, J. M. (2008). Evolution of binding sites for zinc and calcium ions playing structural roles. *Proteins*, **71**, 813–830.
2. Auld, D. S. (2001). Zinc coordination sphere in biochemical zinc sites. *Biometals*, **14**, 271–313.
3. Galperin, M. Y. & Koonin, E. V. (2012). Divergence and convergence in enzyme evolution. *J. Biol. Chem.* **287**, 21–28.
4. Glasner, M. E., Gerlt, J. A. & Babbitt, P. C. (2006). Evolution of enzyme superfamilies. *Curr. Opin. Chem. Biol.* **10**, 492–497.
5. Nagano, N., Orengo, C. A. & Thornton, J. M. (2002). One fold with many functions: the evolutionary relationships between TIM barrel families based on their sequences, structures and functions. *J. Mol. Biol.* **321**, 741–765.
6. Seibert, C. M. & Raushel, F. M. (2005). Structural and catalytic diversity within the amidohydrolase superfamily. *Biochemistry*, **44**, 6383–6391.
7. Baker, P. J., Britton, K. L., Fisher, M., Esclapez, J., Pire, C., Bonete, M. J. *et al.* (2009). Active site dynamics in the zinc-dependent medium chain alcohol dehydrogenase superfamily. *Proc. Natl Acad. Sci. USA*, **106**, 779–784.
8. Fenn, T. D., Ringe, D. & Petsko, G. A. (2004). Xylose isomerase in substrate and inhibitor michaelis states: atomic resolution studies of a metal-mediated hydride shift. *Biochemistry*, **43**, 6464–6474.
9. Kleifeld, O., Frenkel, A., Martin, J. M. & Sagi, I. (2003). Active site electronic structure and dynamics during metalloenzyme catalysis. *Nat. Struct. Biol.* **10**, 98–103.
10. Pauly, T. A., Ekstrom, J. L., Beebe, D. A., Chrunyk, B., Cunningham, D., Griffor, M. *et al.* (2003). X-ray crystallographic and kinetic studies of human sorbitol dehydrogenase. *Structure*, **11**, 1071–1085.
11. Sendovski, M., Kanteev, M., Ben-Yosef, V. S., Adir, N. & Fishman, A. (2011). First structures of an active bacterial tyrosinase reveal copper plasticity. *J. Mol. Biol.* **405**, 227–237.

12. Yoshida, H., Yamaji, M., Ishii, T., Izumori, K. & Kamitori, S. (2010). Catalytic reaction mechanism of *Pseudomonas stutzeri* L-rhamnose isomerase deduced from X-ray structures. *FEBS J.* **277**, 1045–1057.
13. Aharoni, A., Gaidukov, L., Yagur, S., Toker, L., Silman, I. & Tawfik, D. S. (2004). Directed evolution of mammalian paraoxonases PON1 and PON3 for bacterial expression and catalytic specialization. *Proc. Natl Acad. Sci. USA*, **101**, 482–487.
14. Ben-David, M., Elias, M., Filippi, J. J., Dunach, E., Silman, I., Sussman, J. L. & Tawfik, D. S. (2012). Catalytic versatility and backups in enzyme active sites: the case of serum paraoxonase 1. *J. Mol. Biol.* **418**, 181–196.
15. Amitai, G., Gaidukov, L., Adani, R., Yishay, S., Yacov, G., Kushnir, M. *et al.* (2006). Enhanced stereoselective hydrolysis of toxic organophosphates by directly evolved variants of mammalian serum paraoxonase. *FEBS J.* **273**, 1906–1919.
16. Khersonsky, O. & Tawfik, D. S. (2006). The histidine 115-histidine 134 dyad mediates the lactonase activity of mammalian serum paraoxonases. *J. Biol. Chem.* **281**, 7649–7656.
17. Otto, T. C., Harsch, C. K., Yeung, D. T., Magliery, T. J., Cerasoli, D. M. & Lenz, D. E. (2009). Dramatic differences in organophosphorus hydrolase activity between human and chimeric recombinant mammalian paraoxonase-1 enzymes. *Biochemistry*, **48**, 10416–10422.
18. Gupta, R. D., Goldsmith, M., Ashani, Y., Simo, Y., Mullokandov, G., Bar, H. *et al.* (2011). Directed evolution of hydrolases for prevention of G-type nerve agent intoxication. *Nat. Chem. Biol.* **7**, 120–125.
19. Goldsmith, M., Ashani, Y., Simo, Y., Ben-David, M., Leader, H., Silman, I. *et al.* (2012). Evolved stereoselective hydrolases for broad-spectrum G-type nerve agent detoxification. *Chem. Biol.* **19**, 456–466.
20. Karimaki, J., Parkkinen, T., Santa, H., Pastinen, O., Leisola, M., Rouvinen, J. & Turunen, O. (2004). Engineering the substrate specificity of xylose isomerase. *Protein Eng. Des. Sel.* **17**, 861–869.
21. Patel, D. H., Cho, E. J., Kim, H. M., Choi, I. S. & Bae, H. J. (2012). Engineering of the catalytic site of xylose isomerase to enhance bioconversion of a non-preferential substrate. *Protein Eng. Des. Sel.* **25**, 331–336.
22. Harding, M. M., Nowicki, M. W. & Walkinshaw, M. D. (2010). Metals in protein structures: a review of their principal features. *Crystallogr. Rev.* **16**, 247–302.
23. Harel, M., Aharoni, A., Gaidukov, L., Brumshtein, B., Khersonsky, O., Meged, R. *et al.* (2004). Structure and evolution of the serum paraoxonase family of detoxifying and anti-atherosclerotic enzymes. *Nat. Struct. Mol. Biol.* **11**, 412–419.
24. Kuo, C. L. & La Du, B. N. (1998). Calcium binding by human and rabbit serum paraoxonases. Structural stability and enzymatic activity. *Drug Metab. Dispos.* **26**, 653–660.
25. Hartleib, J., Geschwindner, S., Scharff, E. I. & Ruterjans, H. (2001). Role of calcium ions in the structure and function of the di-isopropylfluorophosphatase from *Loligo vulgaris*. *Biochem. J.* **353**, 579–589.
26. Muthukrishnan, S., Shete, V. S., Sanan, T. T., Vyas, S., Oottikkal, S., Porter, L. M. *et al.* (2012). Mechanistic insights into the hydrolysis of organophosphorus compounds by paraoxonase-1: exploring the limits of substrates tolerance in a promiscuous enzyme. *J. Phys. Org. Chem.* **25**, 1247–1260.
27. Carrell, H. L., Glusker, J. P., Burger, V., Manfre, F., Tritsch, D. & Biellmann, J. F. (1989). X-ray analysis of D-xylose isomerase at 1.9 Å: native enzyme in complex with substrate and with a mechanism-designed inactivator. *Proc. Natl Acad. Sci. USA*, **86**, 4440–4444.
28. Lavie, A., Allen, K. N., Petsko, G. A. & Ringe, D. (1994). X-ray crystallographic structures of D-xylose isomerase–substrate complexes position the substrate and provide evidence for metal movement during catalysis. *Biochemistry*, **33**, 5469–5480.
29. Whitlow, M., Howard, A. J., Finzel, B. C., Poulos, T. L., Winborne, E. & Gilliland, G. L. (1991). A metal-mediated hydride shift mechanism for xylose isomerase based on the 1.6 Å *Streptomyces rubiginosus* structures with xylitol and D-xylose. *Proteins*, **9**, 153–173.
30. Kovalevsky, A. Y., Hanson, L., Fisher, S. Z., Mustyakimov, M., Mason, S. A., Forsyth, V. T. *et al.* (2010). Metal ion roles and the movement of hydrogen during reaction catalyzed by D-xylose isomerase: a joint x-ray and neutron diffraction study. *Structure*, **18**, 688–699.
31. Garcia-Viloca, M., Alhambra, C., Truhlar, D. G. & Gao, J. (2002). Quantum dynamics of hydride transfer catalyzed by bimetallic electrophilic catalysis: synchronous motion of Mg(2+) and H(–) in xylose isomerase. *J. Am. Chem. Soc.* **124**, 7268–7269.
32. Garcia-Viloca, M., Alhambra, C., Truhlar, D. G. & Gao, J. (2003). Hydride transfer catalyzed by xylose isomerase: mechanism and quantum effects. *J. Comput. Chem.* **24**, 177–190.
33. Takeda, K., Yoshida, H., Izumori, K. & Kamitori, S. (2010). X-ray structures of *Bacillus pallidus* D-arabinose isomerase and its complex with L-fucitol. *Biochim. Biophys. Acta*, **1804**, 1359–1368.
34. Gonzalez, J. M., Buschiazzo, A. & Vila, A. J. (2010). Evidence of adaptability in metal coordination geometry and active-site loop conformation among B1 metallo-beta-lactamases. *Biochemistry*, **49**, 7930–7938.
35. Solomon, A., Akabayov, B., Frenkel, A., Milla, M. E. & Sagi, I. (2007). Key feature of the catalytic cycle of TNF-alpha converting enzyme involves communication between distal protein sites and the enzyme catalytic core. *Proc. Natl Acad. Sci. USA*, **104**, 4931–4936.
36. Khersonsky, O. & Tawfik, D. S. (2010). Enzyme promiscuity: a mechanistic and evolutionary perspective. *Annu. Rev. Biochem.* **79**, 471–505.
37. Afriat-Jurnou, L., Jackson, C. J. & Tawfik, D. S. (2012). Reconstructing a missing link in the evolution of a recently diverged phosphotriesterase by active-site loop remodeling. *Biochemistry*, **51**, 6047–6055.
38. Elias, M. & Tawfik, D. S. (2012). Divergence and convergence in enzyme evolution: parallel evolution of paraoxonases from quorum-quenching lactonases. *J. Biol. Chem.* **287**, 11–20.

39. Heinz, U. & Adolph, H. W. (2004). Metallo-beta-lactamases: two binding sites for one catalytic metal ion? *Cell. Mol. Life Sci.* **61**, 2827–2839.
40. Tokuriki, N., Jackson, C. J., Afriat-Jurnou, L., Wyganowski, K. T., Tang, R. & Tawfik, D. S. (2012). Diminishing returns and tradeoffs constrain the laboratory optimization of an enzyme. *Nat. Commun.* **3**, 1257.
41. Tawfik, D. S. (2010). Messy biology and the origins of evolutionary innovations. *Nat. Chem. Biol.* **6**, 692–696.
42. Otwinowski, Z. & Minor, W. (1997). Processing of X-ray diffraction data collected in oscillation mode. *Methods Enzymol.* **276**, 307–326.
43. McCoy, A. J., Grosse-Kunstleve, R. W., Adams, P. D., Winn, M. D., Storoni, L. C. & Read, R. J. (2007). Phaser crystallographic software. *J. Appl. Crystallogr.* **40**, 658–674.
44. Murshudov, G. N., Vagin, A. A. & Dodson, E. J. (1997). Refinement of macromolecular structures by the maximum-likelihood method. *Acta Crystallogr., Sect. D: Biol. Crystallogr.* **53**, 240–255.
45. Emsley, P. & Cowtan, K. (2004). Coot: model-building tools for molecular graphics. *Acta Crystallogr., Sect. D: Biol. Crystallogr.* **60**, 2126–2132.
46. DeLano, W. L. The PyMOL Molecular Graphics System. DeLano Scientific LLC. San Carlos, CA, USA. http://www.pymol.org.
47. Humphrey, W., Dalke, A. & Schulten, K. (1996). VMD: visual molecular dynamics. *J. Mol. Graphics*, **14**, 27–28.
48. Nienhaus, G. U. (2005). *Protein–Ligand Interactions: Methods and Applications.* Humana Press, Totowa, New Jersey.
49. Allen, P. & Tildesley, D. J. (1989). *Computer Simulation of Liquids.* Oxford University Press, USA.
50. Hess, B., Kutzner, C., van der Spoel, D. & Lindahl, E. (2008). GROMACS 4: algorithms for highly efficient, load-balanced, and scalable molecular simulation. *J. Chem. Theory Comput.* **4**, 435–447.